CHAPTER 2

2. LITERATURE REVIEW:

2.1. INTRODUCTION:

Coal and petroleum based fossil fuels are rapidly depleting and their utilization is causing release of toxic and greenhouse gases into the atmosphere and in turn leading to severe environmental pollution and global warming. It has been ascertained that the burning of fossil fuels is largely responsible for the increased level of carbon dioxide(CO_2) in the earth's atmosphere (~3×10^{12} kg C yr^{-1}) (Watson et al; 2001). The presence of increasing amount of CO_2 in the atmosphere has resulted in an increase in the average temperature of the earth. Further the CO_2 solubility in ocean water decreases with increase in the water temperature (average decrease ~3%/K).Once the water temperature reaches a critical value, the CO_2 solubility equilibrium shifts towards the gas phase (i. e. air). As a result, there is an additional increase in the atmospheric CO_2 level, leading to further increase in the global average temperature (Zuttel et al; 2004; Sharma et al; 2015). Therefore, it has become extremely necessary to investigate alternate energy sources which have a longer life and are environmentally more benign.

Hydrogen is being considered as the cleanest fuel option for the future (Turner et al; 2004; Mario et al; 2010; Chen et al; 2010). The termHydrogen Economy was coined by John Bockris in 1970 and since then, the idea has gained rapid prominence due to the exceptionally high mass based energy density of hydrogen. Further, it can be stored and transported easily and burns cleanly giving water as the only byproduct (Le et al; 2014). Hydrogen can be suitably exploited as the energy carrier in different sectors to minimize the emission of various harmful gases. Apart from being a clean energy source, hydrogen also has a high calorific value of 122kJ g^{-1} (Han et al; 2004) and hence, it is being considered as the perfect candidate to replace

petroleum fuel (Lee et al; 2012). Internal combustion engine in motorized vehicles can be effectively modified to run entirely on hydrogen or using mixture of hydrogen and natural gas (Chiriac et al; 2015; Anstrom et al; 2016; Hairuddin et al; 2014). Alternatively the engine can be replaced by hydrogen-fuel cells and electrical drives. Such fuel cells are capable of utilizing the chemical energy of H_2 to efficiently produce electricity (Mehta et al; 2003; Winter et al; 2014). Fuel cells running on hydrogen derived from renewable sources are far more environmentally benign than conventional combustion engines, which utilize fossil fuels (Hotza et al; 2001). Fuel-cell technology can revolutionize the existing transportation system as well as conform to the stringent exhaust gas emission guidelines (Li et al; 2000).

Besides use in hydrogen-powered IC engines and fuel cells, there are many other domestic and industrial sectors, where hydrogen has large applications (Watson et al; 2001; Zuttel et al; 2004; Midilli et al; 2005; Balat et al; 2005; Edwards et al; 2008). Hydrogen finds use in petroleum refining (Barreto et al; 2003; Mueller et al; 2007), ammonia synthesis *via* Haber-Bosch process (Ramachandran et al; 1998; Lattin et al; 2007), and refining of metals such as nickel (Ni), tungsten (W), molybdenum (Mo), copper (Cu), zinc (Zn), lead (Pb) and uranium (U) (Eliezer et al; 2000; Eliaz et al; 2000). Hydrogen is also used in the manufacturing of nitrogenous fertilizers, in hydro-desulfurization and hydro-treating of petroleum products, for hydrogenation of hazardous wastes (PCBs, dioxins etc.), in chemical industries and food processing units, for the synthesis of ethanol, methanol and dimethyl ether, for the preparation of alternate fuels *via* Fischer-Tropsch synthesis (gas-to-liquid technology), and as a fuel for high temperature industrial furnaces, among many other applications (Sharma et al; 2015; Dupont et al; 2007)**.** Therefore, developing efficient, cost-effective and eco-friendly means of hydrogen production is highly imperative.

Hydrogen may be produced by implementing technologies based on renewable feed-stocks such as water splitting and biogas reforming (Le et al; 2014; Hotza et al; 2008). In water splitting, hydrogen is generated by breaking the bonds between oxygen and hydrogen through various methods such as electrolysis, photo-catalysis and photo-electrochemical splitting (Le et al; 2001; Maeda et al; 2006; Holladay et al; 2009; Xie et al; 2013; Ji et al; 2013; Xie et al; 2013). Photo-electrochemical (PEC) water splitting requires a PEC cell, which has an anode coated with a photo-catalyst, a cathode coated with an electro-catalyst and an electrolyte. The process generates electron-hole pairs which carry out the respective reduction and oxidation reactions (Antoniadou et al; 2014; Hamann et al; 2014; Zhang et al; 2014; Wang et al; 2014). Electrolysis and photo-catalysis also proceed in a similar fashion, although the respective mechanisms are triggered by different stimuli. Bio-ethanol is produced from biomass (mainly agricultural byproducts and hence, renewable) and which in turn is used to produce hydrogen (Oakley, et al; 2010; Khila et al; 2013; Cormos et al; 2014). However, neither of these technologies can be currently implemented for hydrogen production on a large scale. In fact, electrolysis-assisted water splitting contributes to only about 4% of the total global hydrogen production (Dunn, et al; 2002; De et al; 2007; Zeng et al; 2010). Hence, at present, hydrogen is predominantly produced by steam reforming of naphtha and natural gas and by gasification of coal, heavy oils and petroleum coke (Zeng et al; 2010). Steam reforming of methane is currently the most widely used method for hydrogen production (Le et al; 2014; Centi et al; 2007). In this process, methane and steam react to produce H_2 and CO. Using the gaseous mixture of CO and H_2 in fuel cells is not possible as the presence of CO leads to poisoning of the platinum electrodes and subsequently, results in their inactivation (Centi et al; 2007; Dagle et al; 2007; Wee et al; 2006; Farrauto et al; 2007). The undesirable CO can be removed from the gaseous mixture by employing techniques such as preferential oxidation (PROX), pressure swing adsorption (PSA),

water gas shift reaction (WGSR), etc. (Kim et al; 2013; Jardim et al; 2015; Song et al; 2015; Newson et al; 2007; Tanaka et al; 2003; Shinde et al; 2013; Lee et al; 2009).

This section focuses on the water gas shift reaction and aims to provide a detailed description of the process along with a comprehensive and critical assessment of the efficacy of the catalysts that have been traditionally used to facilitate the reaction. Furthermore, it also attempts to give an idea about how the WGS catalysts have evolved in terms of their structure and performance over the years and provides a futuristic picture of the research required in this area.

Water gas, also known as synthesis gas, contains carbon monoxide (CO) and hydrogen (H_2). Water gas shift (WGS) reaction is the intermediate step used for CO reduction and hydrogen enrichment in the synthesis gas (Byron et al; 2010). In 1780, Italian physicist Felice Fontana discovered the water gas shift reaction, but its actual importance was realized much later.

Steam reforming process yields a gaseous mixture which primarily contains hydrogen, together with appreciable amounts of CO. This CO is further converted using WGS reaction to produce additional hydrogen (Le et al; 2014). Essentially, a mixture of CO and steam is converted to CO_2 and H_2 *via* this step as given below:

$$CO + H_2O \leftrightarrow CO_2 + H_2 \qquad \Delta H^0_{298} = -41.09 \text{ kJ/mol} \qquad (2.1)$$

This reaction [equation (2.1)] is moderately exothermic and its equilibrium constant decreases with increasing temperature. The reaction is favored thermodynamically at lower temperatures and kinetically at elevated temperatures, but is unaffected by changes in pressure (Byron et al; 2010). The water gas synthesis (WGS) reaction is an important process to produce CO-free hydrogen or to adjust the H_2/CO ratio (Soria et al; 2014). Adjusting the H_2/CO ratio is especially required for downstream processes, such as Fischer-Tropsch reactions and methanol

synthesis (Jianlin et al; 2012). It has been reported that the iron catalyst used in ammonia production and the platinum electrode used in fuel-cells are poisoned by the presence of CO (Cameron et al; 2003; Abbas et al; 2010). Therefore, WGS reaction is employed to make reformates free from CO and produce pure hydrogen for use in low-temperature fuel cells and ammonia synthesis plants (Boisen et al; 2010; Jacobs et al; 2004; Sun et al; 2005; Olympiou et al; 2007).

2.2. Water Gas Shift Reaction Catalysts:

In order to achieve large-scale hydrogen production from syn-gas, an appropriate catalyst must be chosen to facilitate the reaction. Figure 1 shows a broad classification of catalysts commonly used for WGS reaction. Various WGS catalysts may be divided into five broad categories: high-temperature, low-temperature, ceria and noble metal based, carbon based, and nano-structured catalysts. Some of the characteristics of common to all WGS catalysts include available oxygen vacancies, activity for the dissociation of water, and low CO adsorption strength (Ammal et al; 2013).

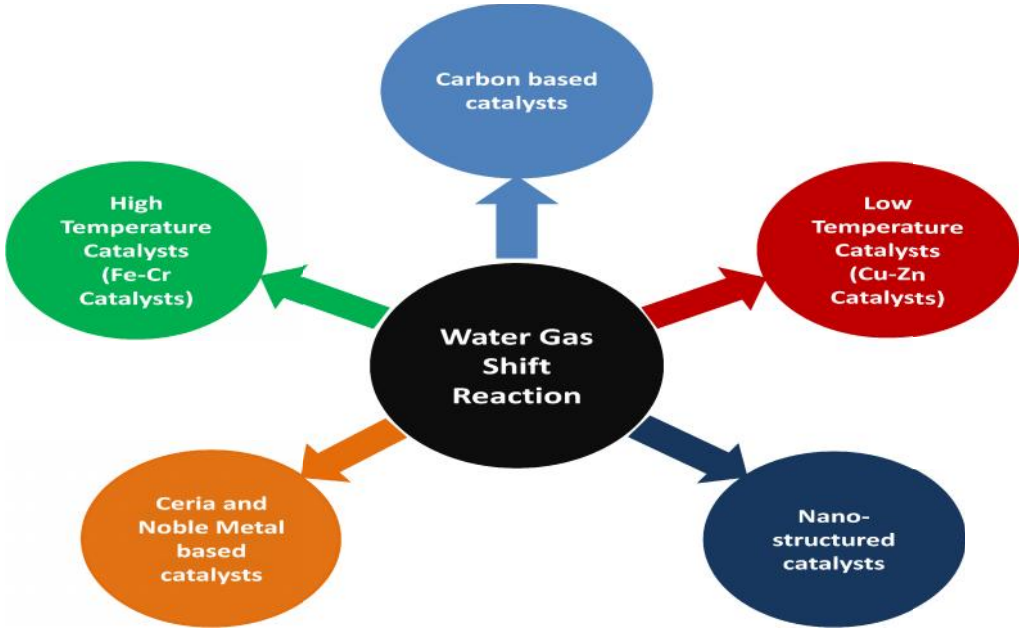

Figure 2.1 Classifications of Catalysts for Water Gas Shift Reaction

The WGS reaction can be catalyzed by both metals and metal oxides alike. In earlier days, conventional iron oxide-chromium oxide catalysts were used in ammonia synthesis plants and were capable of producing an exit composition of 2-4% CO (Twigg et al; 1989). But these catalysts could work only at elevated temperatures (310 to 450 ^{0}C) and hence, they were named as high temperature shift (HTS) catalysts. These catalysts lose their activity significantly at lower temperatures. Therefore, to bring CO levels down to less than 1%, multiple beds with intersystem cooling were necessary (Byron et al; 2010). Much later, copper based catalysts were introduced to operate at much lower temperatures (~200^{0}C). The subsequent CO exit concentrations were brought down to about 0.1-0.3% (Byron et al; 2010). These catalysts came to be known as low temperature shift (LTS) catalysts.

Table 2.1 presents a summary of the available published work in the open literature on the development of various types of WGS reaction catalysts. It includes the general name of the catalyst, methods used for its preparation together with the operating conditions employed, physical characteristics of the prepared catalyst and the specific conclusions drawn regarding the nature of the catalyst and its efficiency. It is seen that a wide variety of catalysts have been developed with the aim of reducing cost of manufacture and improving catalyst efficiency/activity for WGS reaction. A critical discussion highlighting the characteristics of each type of WGS catalysts is also presented in the section following Table 2.1.

Table 2.1 Catalysts used in Water Gas Shift Reaction

Name of catalyst	**Precursor**	**Method/operating conditions**	**Characteristics**	**Remarks/Results**	**Ref.**
High Temperature Shift Catalysts (Iron based WGS catalysts)					
Fe_2O_3	SiO_2, TiO_2, and MgO	**Co-precipitation:** 1:1 (molar) $FeSO_4.7H_2O$ and $Fe_2(SO_4)_3$. $5H_2O$ were dissolved in water, NH_4OH was added, stirred for 30 min, dried at 110^0C, calcined at 400^0C for 2.5 hrs **Incipient Wet-Impregnation:** Fe_2O_3 / support = 30 wt. %, dried at 80^0C, calcined at 400^0C for 2.5 hrs	Fe_2O_3: S. A.-25 m^2/g Fe_2O_3/SiO_2: S.A.- 90.7 m^2/g Fe_2O_3/TiO_2: S.A.-14 m^2/g Fe_2O_3/MgO: S.A.-2.2 m^2/g	The catalytic activity is largely influenced by the acid/base properties of the catalyst. Order of activity: Fe_2O_3/MgO>> Fe_2O_3/TiO_2 >> Fe_2O_3/SiO_2. At a temp of 450^0C, the catalytic activity of basic Fe_2O_3/MgO was reported to be 100 times higher than that of acidic Fe_2O_3/SiO_2.	(Boudjemaa et al; 2011)
Zn-$NiFe_2O_4$	Nitrates of Zn, Ni and Fe(III)	**Co-precipitation:** 2.5M NaOH, pH = 8.5, dried at 110^0C for 24 hrs	Zn (5.7 wt. %) / Ni (31.8 wt. %) / Fe	Zinc enhanced the catalytic activity (CO conversion-	(Lee et al; 2012)

		and calcined at 500^0C for 5 hrs	S. A.= 55 m^2/g	65%, 400^0C). Methanation was also significantly suppressed.	
Ba-promoted Fe_2O_3-Al_2O_3-NiO	Nitrates of Al, Ba, Fe, and Ni	**Co-precipitation:** pH = 10, reflux at 60^0C for 5hrs, drying at 90^0C for 24hrs, calcinations at 400^0C for 4 hrs	Pore volume= 0.3 m^3/g, Pore size= 4.4 nm, S. A. = 165.5 m^2/g, Particle size= 6.8 nm.	Higher activity and stability compared to commercial Cr-catalyst, adding Ba resulted in significant suppression of methanation.	(Meshkani et al; 2015)
Low temperature shift catalysts (Copper based WGS catalysts)					
Cu-Mn spinel oxide	Nitrates copper and manganese	Cu/(Cu+Mn) = 0.3 (atomic ratio) **Single-step Urea-combustion:** Urea undergoes auto-ignition in an open muffle furnace (preheated at 400-500^0C), powder is further calcined at 550^0C for1 hr.	CuMnCB: S.A. = 8 m^2/g CuMn CP: S. A. = 5.9 m^2/g	Due to the higher resistance of copper particles to sintering, CuMn CB was found to be more stable and catalytically active (95% CO conversion at 180^0C) than CuMn CP.	(Tabakova et al; 2013)

		Co-precipitation: copper nitrate was mixed with Na_2CO_3 at 80^0C, pH 8.3; aging time was 6 hrs,Mn nitrate dried at 100^0C, calcined at 700^0C for 7 hrs.??			
$La_{2-x}Ca_xCuO_4$	Nitrates of lanthanum, copper and calcium	**Co-precipitation:** Na_2CO_3/NaOH solution, pH=10, washing-4 hrs, washed with alcohol, dried- 85^0C, 24 hrs, pre-calcined- 350^0C, 2 hrs, calcined- 700^0C, 4 hrs, air flow rate- 50 mL/min X = 0, 0.05, 0.1, 0.15 and 0.20 Reaction temperature = 290^0C	Surface area: 6-18 m^2/g	Best catalytic activity was observed for $La_{1.85}Ca_{0.15}CuO_4$, whereas the best TOF (turnover frequency) values were observed for samples with 5% and 10% calcium. the promoter effect of calcium, a high surface area and the presence of different copper species.	(Maluf et al; 2012)

Cu/ZrO_2, Cu/MgO, Cu/Al_2O_3 and Cu/CeO_2	Nitrates of magnesium and cerium, zirconyl nitrate and Al_2O_3	**Incipient Wet-Impregnation:** Calcined at 400^0C for 6 hrs, Cu loading = 20 wt. %. Gas hour space velocity (GHSV) =36201 h^{-1}	**Cu/CeO_2**: *Impregnated*: S. A. = 106.5 m^2/g, Cu=6.6%, Cu size=15.1 nm, *Co-precipitated*: S. A. = 119.3 m^2/g, Cu=8.5%, Cu size=11.8 nm **Cu/ZrO_2**: S. A. = 152.6 m^2/g, Cu=2.1%, Cu size=47.6 nm **Cu/MgO: S. A.** =157 m^2/g, Cu=2.4%, Cu size= 41.6 nm; **Cu/Al_2O_3: S. A.** = 163.4 m^2/g, Cu=2.9%, Cu size= 34.4 nm CeO_2: 12.8 nm (impregnation) and 5.4 nm (CP);	Cu/CeO_2 catalyst exhibited the highest CO conversion with easier reducibility in WGS. Cu-CeO_2 produced via co-precipitation /digestion method showed better activity and thermal stability than that prepared through impregnation technique.	(Jeong et al; 2014)

			MgO: 15.2 nm; Al_2O_3: 3.6 nm		
CuO/ZrO_2	Copper: copper nitrate ZrO_2: $ZrOCl_2$ and Urea	**Hydrothermal Homogenous Precipitation - ZrO_2 :** autoclaved at 150^0C for 6 hrs, dried at 120^0C and calcined at 350^0C for 4 hrs **Deposition/Precipitation - CuO/ZrO_2:** Cu loadings: 4.1, 6.1 and 8.4 wt. %, ZrO_2, heated at 60^0C, pH-9, aging time-1 hr, aging temp-60^0C, dried at 120^0C and calcined at 400^0C for 4 hrs. 4.1CZ, 6.1CZ and 8.4CZ. Leached with 0.5M ammonium	ZrO_2 support: S. A. = 111 m^2/g 4.1CZ: S. A. = 87 m^2/g, 90.5% (Cu dispersion) 6.1CZ: S. A. = 85 m^2/g, 79.4% (Cu dispersion) 8.4CZ: S. A. = 81 m^2/g, 52.9% (Cu dispersion)	a) Highly dispersed CuO, weakly bound with ZrO_2 b) Strongly bound Cu-[O]-Zr, which can't be leached with ammonium carbonate solution (perhaps related to the surface oxygen vacancy of ZrO_2) c) Crystalline CuO Metallic copper derived from Cu-[O]-Zr species (after H_2-pretreatment) is possibly the catalytically active species for WGSR. Reactivity of the surface hydroxyl	(Zhang et al; 2014)

		carbonate solution for 20 hrs, filtered and washed till pH=7, dried at 120^0C		groups was enhanced by the Cu-[O]-Zr species.	
Ceria and Noble Metal based Catalysts					
Au/Fe_2O_3	$HAuCl_4$	**Double impregnation method (DIM):** Support impregnated with aq. $HAuCl_4.3H_2O$, then with aq. Na_2CO_3, slurry washed and dried at 120^0C; **Liquid phase reductive deposition (LPRD):** $HAuCl_4$ mixed with NaOH in 1:4 weight ratio, aged for 24 hrs (dark), support was added, ultrasonically dispersed for 30 min, and the product aged at 100^0C overnight.	Au loading: 1.5, 3 and 5 wt. %	For the DP, LPRD series, excellent dispersion of gold nanoparticles (2.2-3.1 nm) over the iron oxide surface was observed. Gold nanoparticles promoted reducibility of Fe_2O_3 support and thus enhanced the catalytic activity of the system. The DP synthesized catalyst exhibited the highest enhancement in CO conversion percentage.	(Soria et al; 2014)

		Deposition-precipitation (DP): $HAuCl_4$ mixed with NaOH at pH 9, α-Fe_2O_3 support was added and stirred at 70^0C for 1 hr, product filtered, washed and vacuum-dried at room temperature.			
Au/CeO_2, Au/ZrO_2, Au/CeO_2-ZrO_2	Zirconium tetrachloride, cerium nitrate, $HAuCl_4.3H_2O$	**Precipitation:** For pure ceria and zirconia supports, K_2CO_3 was added at pH 9, temp: 333K (ceria), 353K (zirconia), calcined at 673K (ceria) and 773K (zirconia) **Co-precipitation:** For mixed CeO_2-ZrO_2 supports, wt. ratios = 80:20 and 50:50, K_2CO_3 was added at pH 9, temp: 353K, aging	Ceria: S.A.= 88 m^2/g; CeZr (80:20): S.A.= 114 m^2/g; CeZr (50:50): S.A. = 112 m^2/g	Addition of gold nanoparticles to ZrO_2-modified ceria support enhanced the catalytic activity for WGSR: $AuCe_{50}Zr_{50}$> $AuCe_{80}Zr_{20}$>AuCe. The $AuCe_{50}Zr_{50}$ catalyst exhibited highest activity and stability due to high percentage of gold dispersion, along with favorable	(Phatak et al; 2007)

		time: 2 hrs, filtered, washed and dried in vacuum at 353K, calcined at 673K for 2 hrs **Deposition-Precipitation (DP):** pH=7, temperature: 333K, aging time: 1 hr, washed and dried in vacuum at 353K, calcined at 673K for 2 hrs, Au loading= 3 wt. %		modifications to the acid/base surface properties of ceria.	
$Cu\text{-}CeO_2\text{-}La_2O_3$ (CE09)	Ammonium cerium (IV) nitrate, lanthanum nitrate, $Cu(NO_3)_2.2.5H_2O$	**Urea gelation Co-precipitation (UGC):** Cu loading-10 at.%, Ce/La (atomic ratio) = 2.33 and La/Cu=2.70, heated to 100^0C with stirring, temperature maintained along with periodic addition of water for 8 hrs, filtered,	Particle crystallite size ~ 10.5 nm Size of clusters/agglomerates = 10-100 µm	CO concentration level in the inlet gas enhanced the performance of CE09 at both the temperatures. Reverse WGS reaction was less prominent with CE09 compared to	(Morpeth et al; 2013)

		washed and dried at 100^0C, calcined at 650^0C for5 hrs, Tested for catalytic activity at 550 and 600^0C		commercial Fe-based HT catalysts and Cu-based LT catalysts. At H_2O: carbon ratio greater than 1.5, increasing H_2O concentration had little effect on the rate of WGSR over CE09.	
Pt/CeO_2, Pt/ZrO_2 and $Pt/Ce_{(1-x)}Zr_xO_2$	Zirconyl nitrate, cerium nitrate, $Pt(NH_3)_4(NO_3)_2$	**Co-precipitation/digestion:** $Ce_{(1-x)}Zr_xO_2$ supports were prepared, x= 0.2, 0.4, 0.6, 0.8, 15 wt. % KOH added to the aq. solution of nitrate precursors, calcined at 500^0C for 6 hrs; pure CeO_2 and ZrO_2 supports were also prepared in a similar manner **Incipient wet-impregnation:** Pt	Pt/CeO_2: S. A.= 104 m^2/g, Pt dispersion = 37.6; $Pt/Ce_{0.8}Zr_{0.2}O_2$: S. A.= 119 m^2/g, Ptdispersion = 66.9%; $Pt/Ce_{0.6}Zr_{0.4}O_2$: S. A.=171 m^2/g, Pt dispersion = 57%; $Pt/Ce_{0.4}Zr_{0.6}O$	Catalytic activity was influenced by the reducibility of the catalyst and partly depended on the percentage dispersion of Pt nanoparticles. Pt/CeO_2 nanocatalyst exhibited the highest turnover frequency (TOF) and the lowest activation energy, along with stable activity, in a single stage WGS reaction.	(Jeong et al; 2013)

		loading: 1 wt. %, calcined at 500^0C for 6 hrs**,** GHSV= 45515/hr	$_2$: S. A.=199 m^2/g, Pt dispersion = 60.2%; Pt/$Ce_{0.2}Zr_{0.8}O$ $_2$: S. A.=244 m^2/g, Pt dispersion = 55.7%, Pt/ZrO_2: S. A.=262 m^2/g, Pt dispersion = 43.9%	Pt supported on cubic $Ce_{(1-x)}Zr_xO_2$ support exhibited higher TOF than Pt supported on tetragonal $Ce_{(1-x)}Zr_xO_2$ support.	
Cubic Cu-$Ce_{0.8}Zr_{0.2}$ O_2 and tetragonal Cu-$Ce_{0.2}Zr_{0.8}$ O_2	Copper nitrate, cerium nitrate, zirconyl nitrate	**Co-precipitation/digestion:** 20 wt. % copper, 15 wt. % KOH (co-precipitation agent), Temp- 80^0C, pH-10.5, digested for 3 days, precipitate washed with distilled water, air-dried for 24 hrs, dried at 110^0C for 6 hrs,	Cu-$Ce_{0.8}Zr_{0.2}O_2$: S.A=155.7 m^2/g (fresh), 127.1 m^2/g (used), CuO crystallite size= 16 nm, Cu crystallite size= 13 nm,	The cubic Cu-$Ce_{0.8}Zr_{0.2}O_2$ catalyst had a higher concentration of reduced Cu species than the tetragonal Cu-$Ce_{0.2}Zr_{0.8}O_2$ catalyst and hence higher resistance to sintering. Cubic Cu-	(Jeong et al; 2015)

		calcined at 400^0C for 6 hrs GHSV= 72152 / hr	Cu dispersion = 7.8%; Cu-$Ce_{0.2}Zr_{0.8}O_2$: S. A.=246 m^2/g (fresh), 153.8 m^2/g (used), CuO crystallite size= 17 nm, Cu crystallite size= 18 nm, Cu dispersion = 5.6%	$Ce_{0.8}Zr_{0.2}O_2$ exhibited higher CO conversion (17.4% at 320^0C) due to improved oxygen mobility and higher percentage of Cu dispersion.	
Carbon WGS Catalysts					
Na-promoted carbon-supported Pt catalyst	Multi-walled carbon nanotubes (MWCNTs), sodium acetate,	**MWCNT oxidation:** Surface oxidation by 70% nitric acid, reflux at 120^0C for 2 hrs (2h-C_N), washed and dried at 60^0C **Alkali-metal ion**	800-Na-2h-C_N: 160 m^2/g	The catalyst undergoes a mild activation for WGSR due to the nitric acid oxidation of the MWCNTs, prior to platinum addition.	(Zugic et al; 2014)

	$Pt(NH_3)_4.(NO_3)_2$	**exchange and annealing:** 2h-C_N suspended in 1M sodium acetate, refluxed at 60^0C for 24 hrs, washed, dried at 60^0C (Na-2h-C_N), calcined at 800^0C for 2-4 hrs **Incipient wet-impregnation:** 1 wt. % Pt, 0.02g $Pt(NH_3)_4.(NO_3)_2$ added to 1.5 mL deionized water, added drop-wise to support, dried at 60^0C		The incorporation of sodium via ion-exchange increases catalytic activity by altering the surface oxygen distribution.	
CeO_2/AC (activated carbon, AC)	Cerium nitrate hexahydrate	**Direct steam activation (AC support):** AC prepared from olive stones, washed with dil. H_2SO_4 and then with distilled water until no sulfates were detected, dried at 373K for overnight;	AC support particle size = 0.5nm-1nm Ceria particle size = 2-4 nm	Development of highly dispersed ceria nanoparticles on activated carbon. Average particle size was significantly lower than that of unsupported ceria. As a result, the ceria	(Serra no et al; 2008)

		Impregnation (CeO_2/AC): $Ce(NO_3)_2.6H_2O$ is dissolved in acetone, dried AC is added to the solution, kept for 3 days in covered flask followed by slow removal of excess solvent, dried at 373K, overnight, heated at 623K for 5hrs @ 5K/min		particles got placed at the most internal parts of the porous support. Lower average particle size of ceria in CeO_2/AC accounts for its easier reducibility as compared to massive ceria.	
Nano-Structured Catalysts					
Cu/AC, Ni/AC and Cu-Ni/AC	Copper nitrate, nickel nitrate; AC: commercial activated charcoal	**Preparation of AC support:** Commercial AC was mixed with 10 wt. % ethanol, CMC used as binder, heated for 24 hrs, dried at 80^0C for 12 hrs, pyrolyzed at 600^0C for 3 hrs in N_2 flow (25 mL/min) @ 0.5^0C/min	Cu/AC: S.A.= 419 m^2/g, Pore size = 2.9 nm, metal particle size = 25.4 nm; Ni/AC: S.A.= 417 m^2/g, Pore	Catalytic activity increased with increase in the reaction temperature for all prepared catalysts. Cu-Ni (2:1)/AC catalyst exhibited highest activity (99.4% CO conversion), along with satisfactory suppression	(Arbelaez et al; 2015)

		Conventional wet-impregnation: (CuO+NiO) loading = 20 wt. %, Cu:Ni (molar ratio) = 2:1 and 1:2, mixing of precursor solutions with AC pellets, roto-evaporated for 3 hrs, dried at 90^0C for 12 hrs, heated at 500^0C for 3 hrs, reduced in 5% H_2/Ar at 600^0C	size = 2.8 nm, metal particle size = 22.3 nm; Cu-Ni (2:1)/AC: S.A.= 415 m^2/g, Pore size = 3.1 nm, metal particle size = 13.7 nm; Cu-Ni (1:2)/AC: S.A.= 434 m^2/g, Pore size = 2.9 nm, metal particle size = 13.2 nm	of methanation and carbon gasification reactions. Well-suited for use in medium temperature WGS reactions. Cu-Ni (2:1)/AC catalyst's performance was comparable to that of ceria-supported noble metal catalysts. The improved catalytic activity was related to the formation ofCu-Ni alloy as evidenced by XRD and/or to a possible Cu/NiOx active site formation.	
Mn-Cr/TiO_2	Chromium nitrate, manganese nitrate,	**Co-precipitation:** Chromium nitrate: manganese nitrate= 2:3, aging time-6 hrs,	Atomic % (CP) = 14.6 % Mn / 9.7 % Cr;	The Mn-Cr/TiO_2 catalyst prepared by thermal decomposition method was found to	(Farzanfar et al; 2015)

	ammonium thiocyanate (NH_4SCN), TiO_2 (82 m^2/g) $\rightarrow [Mn(H_2O)_6]_3 [Cr(NCS)_6]_2.H_2O/TiO_2$	dried at 120^0C, calcined at 600^0C for 4 hrs **Impregnation:** Aging time- 6 hrs, aging temp-30^0C, dried at 120^0C, calcined at 600^0C for 4 hrs **Thermal decomposition:** Calcination of $[Mn(H_2O)_6]_3 [Cr(NCS)_6]_2.H_2O /TiO_2$ - 600^0C, 4 hrs	Atomic % (IMP) = 14.3 % Mn / 9.5%Cr; Atomic % (TD) = 14.3 % Mn / 10.1%Cr	exhibit smaller particle sizes, higher BET surface area (141.9 m^2/g) and hence, higher catalytic activity (72.6% CO conversion at 320^0C) compared to those synthesized via other methods.	
Metal (M)-modified (M= Cr, Al, Mn, Ce, Ni, Co and Cu) ferrite crystals	Nitrates of iron (III),chromium, aluminium, manganese, cerium, nickel, cobalt and copper	**Co-precipitation:** pH=10, aging time: 5 hrs, dried at 90^0C, calcined at 400, 450 and 500^0C for 4 hrs at 5^0C/min	Surface area: 55.7 to 199.1 m^2/g Particle size: 5.7 to 20.2 nm	Addition of copper favored the active phase formation of the iron oxide catalyst and also resulted in an increase in the specific surface area. Fe-Al-Cu catalyst with Fe/Al=10 and Fe/Cu=5 weight ratios showed highest catalytic	(Meshkani et al; 2015)

				activity. Increasing the steam/gas ratio enhanced the WGS activity, but increasing the GHSV adversely affected the percentage of CO conversion.	
Fe_2O_3-Cr_2O_3-CuO	Nitrates of iron (III), chromium and copper	**Co-precipitation:** 88.8 wt. % Fe_2O_3, 8.88 wt. % Cr_2O_3, 2.32 wt. % CuO, molarity-0.06, 0.12 and 0.24M, pH-7, 8, 9 and 10, aging temp- 40, 60 and 80^0C, aging time- 0.5, 5 and 10 hrs, dried at 90^0C, calcined at 400, 450 and 500^0C for 4 hrs at 5^0C/min	Particle size: 10 to 20 nm Surface area: 28.2 to 91.1 m^2/g	Surface area increased with increase in pH value and decrease in calcination temperature. The catalyst prepared from a precursor solution having a concentration of 0.06M, at pH=10, aging temperature of 60^0C, aging time of 5 hrs, and calcined at 400^0C, exhibited the highest surface area and catalytic activity.	(Meshkani et al; 2015)

Fe_2O_3-Cr_2O_3-CuO	Ferric nitrate, urea, ferrous sulfate, chromium nitrate, copper nitrate	**Modified urea hydrolysis:** 88.8 wt. % Fe_2O_3, 8.88 wt. % Cr_2O_3, 2.32 wt. % CuO, Urea/Fe^{3+} molar ratio=12, pH-11, aging temp-40, 60 and 80^{0}C, aging time-0.5, 5 and 10 hrs, dried at 90^{0}C, calcined at 400, 450 and 500^{0}C for 4 hrs at 5^{0}C/min.	Average crystallite size-less than 15 nm Surface area: 57.58 to 119.48 m^2/g	Surface area increased with increase in pH value and decrease in calcination temperature. For an optimum aging time and aging temperature, the catalyst possessed the highest BET surface area. Satisfactory stability in high temperature WGS reaction.	(Meshkani et al; 2015)
Pt/CeO_2	Platinum acetylacetonate (Ptacac)	**Reactive spray deposition technology (RSDT): Pt nanoparticles:** Xylene : acetone = 3:1, Pt acac-0.6 mM/L, 62.5 wt % Xylene, 21 wt. % acetone, 16.5 wt. % sulfur-free propane, flow rate-4 mL/min, temp-60^{0}C	Platinum: 1 wt % (0.5-2 nm) Ceria: 8-30 nm	Superior activity compared to catalysts prepared through sol-gel, co-precipitation and incipient wetness impregnation methods. 100% CO conversion was achieved at 250^{0}C at a GHSV of 8622 hr^{-1}. Uniform distribution of Pt nanoparticles over the ceria surface and the	(Jain et al; 2014)

		Ceria slurry: 1 wt. % ceria in deionized water, pH-5, ultra-sonication-1 hr, energy input-200-250 kJ, flow rate-1.5 mL/min.		absence of sintering and agglomeration of Pt nanoparticles.	
Pt/CeO_2	Cerium hydroxy carbonate (CHC), $Pt(NH_3)_4.(NO_3)_2$	**Incipient wetness impregnation:** Aging time- 0-8 hrs, pre-calcination temp-400-700^{0}C, Pt: 1 wt. %, calcined at 400^{0}C for 4 hours	400^{0}C: S.A.= 136 m^2/g; 500^{0}C: S.A.= 86 m^2/g; 600^{0}C: S.A.= 24 m^2/g; 700^{0}C: S.A.= 7 m^2/g	The catalyst exhibited the highest CO conversion (~82%) and the lowest activation energy of 55 kJ/mol at a GHSV of 45515 hr^{-1}, when a pre-calcination temperature of 400^{0}C and aging time of 4 hrs was employed in the synthesis of ceria.	(Jeong et al; 2015)
Au/CeO_2-M/Al_2O_3; M: Fe, Cu, Zn	$HAuCl_4$, Nitrates of cerium, iron (III), copper and zinc,	**Conventional co-precipitation (support preparation):** Precursors impregnated on γ-	Au/Ce/Al: S.A.=197 m^2/g, CeO_2 crystallite size = 5.5 nm Au/CeFe/Al:	Catalytic activity of $Au/CeO_2/Al_2O_3$catalyst enhanced by addition of Fe, Cu and Zn to the ceria support. Enhanced redox	(Reina et al; 2015)

	γ-alumina powder	alumina powder in 50 mL ethanol, evaporated, dry solid (at 50^0C), treated with 10M NH_3, filtered, dried and calcined-500^0C, 4 hrs, 15 wt. % Ce-M mixed oxide, 2 wt. % doping metal oxide **Gold deposition via DAE:** Final Au loading: 2 wt. %, support was sieved (100-200 µm fractions retained), dried at100^0C after Au deposition, calcined at 350^0C for 4 hrs	S.A.=184 m^2/g, CeO_2 crystallite size = 5.6 nm Au/CeCu/Al: S.A.=175 m^2/g, CeO_2 crystallite size = 7.3 nm Au/CeZn/Al: S.A.=181 m^2/g, CeO_2 crystallite size = 5.1 nm	properties and structural promotion. Both Cu and Zn enhanced the OSC of the primary support, but Zn was found to be a better redox promoter. However, Fe was the best choice for as dopant, since it functioned both as a redox promoter as well as a structural promoter.	
Pd/Cu/ceria, Pd/CeO_2 and Cu/CeO_2	Cerium nitrate, Copper nitrate, Copper	**Electrospinning:** 12 ml spinning solution, spinneret: -20kV, collector: +2kV, 22cm distance, flow rate-	2 wt. % Pd, 10 wt. % Cu and 88 wt. % CeO_2	Transition metals in the ceria lattice facilitate the reduction of energy barriers for O vacancy formation and thereby	(Gibbons et al; 2014)

	acetate, Copper chloride	1mL/hr, calcinations at 550^0C for 3hrs @ 2^0C/min, calcinations at 150^0C to 250^0C @ 0.1^0C/min.		promote H_2O splitting on the ceria surface. Pd and Cu metal reduction and surface segregation during testing conditions may reduce favorable sites in ceria lattice for vacancy formation.	
Pt/CeO_2	Cerium nitric	**Electrospining (ESP)** /WGSR 2:1(v/v) ethanol/water mixtures as the co-solvent, thermal treatment at 650°C for 3 h	Nanofiber dia. of 80-120 nm, crystal size 5-10 nm particles.	Nanofiber **CO** conversion reaches 98% at 320°C	(Tang et al. 2012)
Cu-CeO_2	Cerium nitrate	**ESP**/ CO PROX Cerium nitric/PVP, 2:1(v/v) ethanol/water mixtures as the co-solvent, followed by thermal treatment at 600°C for 3 h.	Nanofiber dia. 100-200 nm, Dried-18 h at 50 °C , Calcin.- 600 °C for 3 h in air	Nanofiber is an efficient cat. for CO-PROX and the conc. of CO in tail gas can be reduced <100 ppm.	(Xu et al. 2011)

CeO_2-ZnO	zinc acetate and cerium nitrate	**ESP**/ zinc acetate and cerium nitrate, PVP template, and 2:1(v/v) ethanol/water mixtures as the co-solvent, followed by thermal treatment at 600°C for 3 h.	Nanofibers dia. 200-300 nm, Dried-12 h at 60 °C under vacuum, Calcin.- 600 °C for 3 h in air	The CeO_2-ZnO nanofibers possessed a higher photocatalytic activity than that of the pure CeO_2 or ZnO nanofibers for the degradation of dye.	(Li et al. 2011)
Pt-TiO_2	$TiCl_4$/ Ammonia solution	**ESP**/WGSR Ti(OH)n, 25% Pt loaded Ti(OH)n nanoparticle slurry was prepared by a CP calcin.- 773 K , 4 h	Nanofibers dia. 200-900 nm, pH-8.5	Catalytic activity of NFC for WGSR was5-7 times higher than that of BC, effective dispersion of Pt metals in the nanofibers.	(Kim et al. 2009)

2.2.1. High temperature shift catalysts:

The HTS catalysts generally operate in the temperature range of 310 to 450^0C and are called ferrochrome catalysts because of their typical composition (Rhodes et al; 1995).The inlet feed temperature is normally maintained at 350^0C to prevent excessive increase in the temperature inside the reactor, which could possibly damage the catalyst. With this inlet temperature, a maximum outlet temperature of about 550^0C is observed (Byron et al; 2010). Iron-chromium oxide was first patented as a WGS catalyst in 1914 (Bosch et al; 1914). The

typical composition of HTS catalyst is reportedly 74.2% Fe_2O_3, 10.0% Cr_2O_3, 0.2% MgO, and rest being volatiles (Newsome et al; 1980). The Fe/Cr catalyst is usually prepared *via* base-catalyzed co-precipitation of $Fe_2(SO_4)_3$ and $Cr_2(SO_4)_3$ using Na_2CO_3(Lee et al; 2006). Cr_2O_3 acts as a stabilizer and prevents the sintering of Fe_2O_3. Though the optimal content of Cr_2O_3 is reported to be 14% (Newsome et al; 1980), in order to prevent any significant reduction of the surface area, about 8% is used industrially (Rhodes et al; 2002). The outlet concentration of a conventional Fe/Cr WGS reactor can be as low as 3% CO; this is the equilibrium concentration at 450^0C (Byron et al; 2010). Inorganic salts, boron, oils, phosphorus compounds, liquid water (temporary poison), and sulfur compounds in concentrations greater than 50 ppm act as poisons for the iron-chromium catalyst (Rase et al; 1977). The activity of such catalysts gets diminished mostly due to the thermal sintering of the magnetite phase, but during operation, increasing the reaction temperature somewhat compensates for this decrease (Twigg et al; 1989). Due to gradual deactivation, lifetime of an average catalyst is in the range of 3-5 years (Rhodes et al; 1995). The CO to steam ratio is a parameter of utmost importance in HTS reactions, and operating the reaction at high ratios may lead to metallic iron formation, carbon deposition, methanation and Fischer Tropsch reaction (Twigg et al; 1989). A contact time of approximately 3-9 seconds is suggested for the reaction (Callaghan et al; 2003).

Iron catalysts are initially present as α-Fe_2O_3 (hematite) but get reduced to Fe_3O_4 (magnetite) during the reaction, which is reported to be the active phase (Yu et al; 2006). The pre-reduction of Fe_2O_3 to the catalytically active Fe_3O_4 is generally performed at 315-460^0C using the reactant gas (syn gas) (Arnold et al; 1997). To prevent the continued over-reduction into FeO or metallic iron, the *R* factor (reduction factor) of the reactant gas is maintained approximately at 1.0 by adding excess steam (Lee et al; 2009; Rhodes et al; 2002).

The R-factor can be defined by the formula (Byron et al; 2010):

$$R = (\{[CO] + [H_2]\} / \{[CO_2] + [H_2O]\}) \quad (2)$$

The R-factor can be controlled by adjusting the composition of steam in the steam-synthesis gas mixture. Over the years, many improvements have been introduced to iron oxide catalysts. One such improvement is the addition of Cu as a promoter to the Fe/Cr catalyst in order to decrease the activation energy (Rhodes et al; 2003) and increase the selectivity by suppressing methanation (Lee et al; 2006). Another noteworthy advancement has been the addition of a less toxic metal (such as aluminum and cerium) which is capable of giving the high conversion and stability that chromium provides. Though chromium increases the conversion efficiency, it also increases the toxicity and results in higher disposal cost of the spent catalyst. The chromium species in a fresh Fe/Cr catalyst are usually Cr^{3+} with very low amounts of Cr^{6+}. The hexavalent chromium (Cr^{6+}) is water-soluble and may be leached from the catalyst by condensed steam or cold water and can pose a serious threat to the environment due to its carcinogenic nature and toxicity (Pellerin et al; 2000). Ladebeck and Kochloefl (1995) investigated the replacement of Cr in a Fe/Cu/Cr catalyst with Al/Ce. The resulting Fe/Cu/Al/Ce catalyst showed superior catalytic activity than the commercial catalysts. Since then, aluminium has been viewed as a suitable replacement for chromium and numerous studies have been conducted on the incorporation of Al into the iron oxide HTS catalysts. Araujo and Rangel (2000) demonstrated that the activity promoted by the addition of Al becomes more pronounced when Cu is also incorporated into the magnetite matrix. Under low steam-to-gas ratios (*S/G* = 0.4; estimated *R* factor = 0.9), the Fe/Al/Cu catalyst exhibited similar HTS activity but better selectivity (suppressed methanation) than a typical commercial Fe/Cr catalyst. The authors explained the above results by suggesting

that Al/Cu promoted the magnetite phase formation during pre-reduction and stabilized the phase against subsequent reduction to FeO and metallic iron.

Liu et al. (2005) investigated an Al/Ce-promoted iron catalyst (Fe/Al/Ce) and adopted γ-Fe_2O_3 (magnetite) as the backbone of the iron oxide catalyst, because it was thought to be more effective than α- Fe_2O_3 in incorporating promoter elements, by making use of the vacant sites of an imperfect spinel structure (Kundu et al; 1988). It may be deduced that Liu et al. (2005) regarded both Al and Ce as textural promoters for the magnetite phase. They reported the catalyst to be active, thermo-resistant and comparable to a commercial Fe/Cr catalyst in both HTS activity and specific surface area. The Ozkan's group**s** of the Ohio State University have reported extensive work on the Fe/Al/Cu HTS catalyst in the last decade (Natesakhawat et al; 2006; Zhang et al; 2008; Zhang et al; 2009; Gawade et al; 2010). Aluminum has been found to be a suitable replacement for chromium. It has been reported that it functions as a textural promoter by preventing the sintering of iron oxides and stabilizing the magnetite phase. Copper functions as a structural promoter and enhances the catalytic activity by providing additional active sites.

Efforts have also been made to use thorium in place of chromium because it decreases sintering and increases activity and has reduced toxicity. Rangel Costa et al. (2002) replaced chromium with thorium in Fe/Cr/Cu catalysts. As thorium ions (Th^{4+}) are considerably larger than Fe^{3+} ions, Th^{4+} cannot be incorporated into the iron oxide lattice; instead they form a segregated phase on the surface. Subsequently, they stabilize the magnetite phase against further reduction and hence, thorium can be considered as a textural promoter for iron based HTS catalysts. But, an optimum amount must be used because thorium poisons the active sites of the iron. Like aluminium, activity of thorium can also be enhanced by using Cu as a co-promoter. Junior et al. (2005) investigated vanadium (V^{4+}) as a possible replacement for chromium. Though vanadium

cannot be strictly termed as a textural promoter, it does stabilize Fe^{3+} and also increases the activity and selectivity of the magnetite phase, indicating its role as a functional promoter. Boudjemaa et al. (2011) synthesized several chromium-free Fe_2O_3, Fe_2O_3/SiO_2, Fe_2O_3/TiO_2 and Fe_2O_3/MgO catalysts (Table.2.1) and investigated their behavior in high-temperature WGS reaction *via* diffused reflectance infrared Fourier transform spectroscopy (DRIFTS). The Fe_2O_3/SiO_2, Fe_2O_3/TiO_2 and Fe_2O_3/MgO catalysts were prepared by incipient wetness impregnation method, while bulk Fe_2O_3 was synthesized *via* co-precipitation method. At a reaction temperature of 450^0C, the catalytic activity of basic Fe_2O_3/MgO was reported to be 100 times higher than that of acidic Fe_2O_3/SiO_2. The catalytic activity followed the trend: $Fe_2O_3/MgO >> Fe_2O_3/TiO_2 >> Fe_2O_3/SiO_2$. Thus, the authors inferred that the catalytic activity was largely influenced by the acid/base properties of the catalyst. Addition of varied amounts of Cu, Pb, barium (Ba), silver (Ag) or mercury (Hg) showed increased catalytic activity, with the order of activity being Hg > Ag and Ba > Cu >Pb (Rhodes et al; 2002). Particularly, lead (Pb) has been shown to enhance the catalytic activity by several research groups and is often added to Fe/Cr catalysts in miniscule amounts. In high oxidation states, lead and iron react together resulting in higher activity in the WGS reaction (Topsoe et al; 1973).

Nickel is usually thought to be unsuitable for use in WGS catalysts because of its easy reducibility under the given conditions and also because it significantly promotes methanation (Andreev et al; 1986). But it is capable of forming a solid solution with iron oxide to produce a Fe/Ni catalyst with reasonable HTS activity, when promoted by another suitable element (Jianlin et al; 2012).

Lee et al. (2012) investigated the effects of addition of zinc to a $NiFe_2O_4$ catalyst (Table.2.1) used for HTS reaction of natural gas reformates. Ni/Fe exhibited high HTS activity comparable to commercial catalysts, but due to the presence of nickel oxide, methanation also

occurred during HTS catalysis (Lee et al; 2011). With the addition of zinc into inverse-spinel $NiFe_2O_4$, the lattice size increased, the HTS activity improved and methanation got suppressed. Cesium (Cs) was also impregnated on the Ni/Fe catalyst to improve activity and suppress methanation (Lee et al; 2011). Several Fe/Ni/Cs catalysts were tested under a weight hour space velocity (WHSV) of $0.075 m^3/g_{cat}/hr$; whereas Zn promoted Ni/Fe catalysts were tested under a WHSV of $0.035 m^3/g_{cat}/hr$. In both the cases, the respective catalysts showed enhanced activity for WGS reaction with similar levels of improvement, implying that the Ni/Fe/Cs catalyst is superior than the Zn promoted Ni/Fe catalyst in terms of activity enhancement.

Watanabe et al. (2009) studied the effect of incorporation of Al in Ni/Fe catalysts and reported excellent HTS activity and satisfactory methanation suppression. Best performance in terms of catalytic activity and suppression of methanation were observed when Fe/(Fe+Ni) atomic ratio was between 0.5 and 0.8. Watanabe et al. (2011) further developed the idea and tried to suppress methanation over the Ni/Fe species by dispersing Ni/Fe over a mesoporous CeO_2-ZrO_2 support prepared by the "hard-template method". Owing to the large specific surface area of the support and improved transfer rate of lattice oxygen, the prepared catalyst exhibited enhanced thermal stability, HTS activity and suppressed methanation compared to a conventionally prepared catalyst (Lee et al; 2013).

Quite recently, Ba-promoted chromium-free Fe_2O_3-Al_2O_3-NiO catalyst (Table.2.1) was investigated for high temperature WGS reaction (Meshkani et al; 2015). The prepared mesoporous catalyst had a high specific surface area (165.5 m^2/g) and nanosize crystallite particles of 6.8 nm size. These authors reported that the Ba-promoted catalyst exhibited relatively higher activity and stability, along with satisfactory suppression of methanation. The addition of Ba to the Fe_2O_3-Al_2O_3-NiO catalyst gave rise to more basic sites on the surface of the

catalyst, which could promote WGS reaction selectivity against methanation (Hwang et al; 2011).

Single atom doped iron catalysts have also been investigated recently using iridium as the doping atom (Lin et al; 2013). Single atom doping results in increase in activity by an order of magnitude higher than that with nanoparticle doping. Added to this is the fact that this method uses less metal for doping which greatly reduces material costs. This method also leads to enhancement in the Oxygen Storage Capacity (OSC) of the iron supports, thus further facilitating the WGS reaction. Recent investigations on the use of chromium promoted skeletal iron catalysts have also yielded quite encouraging results (Leoni et al; 2011).

2.2.2. Low temperature shift catalysts:

The low temperature shift (LTS) reaction occurs at 200^0C to 250^0C and the common LTS catalyst is a mixture of CuO, ZnO and Al_2O_3/Cr_2O_3(Byron et al; 2010). The typical compositions of such catalysts are reported to be 68-73% ZnO, 15-20% CuO, 9-14% Cr_2O_3, 2-5% Mn, Al and Magnesium oxides(Newsome et al; 1980) and 32-33% CuO, 34-53% ZnO and 15-33% Al_2O_3(Bosch et al; 1914; Callaghan et al; 2003). Recent developments have given rise to catalysts that can operate at medium temperatures of around 300^0C. Copper metal crystallites are the active species in the catalyst. ZnO and Cr_2O_3 provide the structural support for the catalyst and Al_2O_3, though largely inactive, helps in the dispersion and minimizes pellet shrinkage (Byron et al; 2010).

The Cu/Zn catalysts are very sensitive to temperature and are pyrophoric in air (Byron et al; 2010). These catalysts are sulfur, halogen and unsaturated hydrocarbon intolerant and hence need to be protected from these compounds (Rase et al; 1977). The ZnO is effective in reducing the poisoning of copper by sulfur (Twigg et al; 2001). Hence, to prevent the sulfur poisoning, a guard bed of ZnO is always used before the LTS reactor. The CO exit concentration, as low as

0.1%, can be achieved through LTS reactor (Byron et al; 2010). The LTS catalysts are highly selective and thus allow for a high conversion ratio, especially at low intake concentrations (Fu et al; 2005; Chinchen et al; 1988). The normal life time of the low temperature catalyst is 2-3 years (Rase et al; 1977). Tanaka et al. (2003) reported that $CuMn_2O_4$ and $CuAl_2O_4$ catalysts exhibited higher CO conversion efficiencies than the standard commercial catalyst. Also, the copper-ceria (Cu/CeO) catalyst was found to be non-pyrophoric and stable (Kusar et al; 2006). Furthermore, it was shown that employing a Mn promoted Cu/Al_2O_3 catalyst could result in a CO conversion efficiency of about 90% in WGSR (Yeragi et al; 2006).

Tabakova et al. (2013) synthesized Cu-Mn spinel oxide catalysts (Table.2.1) *via*a single step urea-combustion and co-precipitation procedures.They reported higher copper dispersion in the catalysts prepared using combustion method. The catalytic studies revealed that combustion synthesis produced more active and stable Cu-Mn spinel oxide catalysts due to higher resistance of copper particles to sintering (Figueiredo et al; 2010; Gines et al; 1995). Catalysts having perovskite structures have also been investigated recently for LT-WGS reactions. Perovskite-type oxides, of the general formula ABO_3, can act as suitable catalysts due to their high activity and thermal stability (Lisi et al; 1999; Merino et al; 2005). Maluf et al. (2012) studied the effect of addition of small amounts of calcium on the structure and catalytic properties of $La_{2-x}Ca_xCuO_4$ (Table.2.1). All the catalyst samples possessed a well-defined perovskite structure with surface areas ranging between 6 and 18 m^2/g. The best catalytic activity was observed for $La_{1.85}Ca_{0.15}CuO_4$, whereas the best TOF (turnover frequency) values were observed for samples with 5% and 10% calcium. The authors attributed this property to the promoter effect of calcium, higher surface area and presence of different copper species. Jeong et al. (2014) synthesized metal-oxide supported Cu catalysts (Table.2.1) *via* co-precipitation/digestion and incipient wetness impregnation methods. Al_2O_3, ZrO_2, MgO and CeO_2 were studied as the support

materials and the copper loading was maintained at 20 wt. %. It was reported that Cu/CeO_2exhibited the highest copper dispersion and the highest CO conversion in the temperature range between 320 and 400^0C. Moreover, Cu/CeO_2produced *via* co-precipitation/digestion method exhibited appreciably higher CO conversion with easier reducibility in WGS reactions. Furthermore, the catalyst produced *via* this method showed better catalytic activity and thermal stability than that produced through impregnation method.

Zirconia possesses favorable redox properties, high thermal stability (Zhang et al; 2014), adequate number of surface oxygen vacancies (Zhao et al; 2004; Zhang et al; 2012) and surface hydroxyl groups (Pigos et al; 2007; Franchini et al; 2012; Chenu et al; 2005; Graf et al; 2009). Therefore, ZrO_2-supported Cu catalysts have received considerable attention in recent years for use in low temperature WGS reactions(Ko et al; 2005; Aguila et al; 2008; Ruan et al; 2012; Chen et al; 2014; Esposito et al; 2011).

Zhang et al. (2014) prepared a series of CuO/ZrO_2 catalysts (Table.2.1) *via* deposition-precipitation method and evaluated their performance for low-temperature WGS reaction. The catalysts with different amounts of copper loading: 4.1, 6.1 and 8.4 wt. %, were synthesized and hence, were denoted as 4.1CZ, 6.1CZ and 8.4CZ, respectively. To identify the different supported copper oxide species, the catalysts were further leached with 0.5M Na_2CO_3 solution for 20 hrs. Experiments revealed that the as-prepared CuO/ZrO_2 catalysts contained three types of CuO species: (a) highly dispersed CuO (weakly bound with ZrO_2); (b) strongly bound Cu-[O]-Zr, which couldn't be leached with ammonium carbonate solution; and (c) crystalline CuO. At a temperature of 200^0C, the reaction rates of the prepared catalysts followed the sequence: 6.1CZ > 8.4CZ > 4.1CZ. This order was in accordance with the amount of Cu-[O]-Zr species in the CuO/ZrO_2 catalysts. Hence, the authors suggested that the metallic copper derived from Cu-[O]-Zr species (after H_2- pretreatment) are the catalytically active species for WGS reaction. Copper

based catalysts are susceptible to poisoning by sulfur compounds present in the hydrocarbon sources, whereas the iron based catalysts are more robust and sulfur tolerant (Byron et al; 2010). Therefore, the WGS reaction is commercially carried out using two adiabatic stages, the high temperature shift followed by the low temperature shift with intersystem cooling to maintain temperatures at the inlet (Twigg et al; 1989). Also, a guard bed is used prior to the LTS reactor to remove the sulfur compounds and protect the copper catalyst (Byron et al; 2010).

2.2.3. Ceria and Noble Metal based Catalysts:

The commercial iron-chromium HTS catalysts and the copper-zinc LTS catalysts were by and large successful on an industrial scale; however, they possessed certain inherent drawbacks which entailed researchers to look beyond them. For example, in the presence of excess fuel from the reformer, coke formation becomes a constant nuisance for the iron based catalysts (Byron et al; 2010; Wheeler et al; 2004). Also, the Cu catalyst is pyrophoric in its reduced state and gets deactivated in the presence of condensed water due to leaching of active component or formation of surface carbonates (Byron et al; 2010; Kusar et al; 2006; Wheeler et al; 2004; Mhadeshwar et al; 2005). Therefore, much research has already been done and is still being carried out to develop alternative catalysts free from aforementioned drawbacks.

Ceria and CeO_2-based catalysts have the unique combination of an elevated oxygen transport capacity along with the ability to shift easily between reduced and oxidized states (i.e. $Ce^{3+} \leftrightarrow Ce^{4+}$) and this property can be increased with the addition of transition metal ions in the ceria lattice (Pontelli et al; 2011; Roh et al; 2011; Roh et al; 2012). The strong metalsupport interactions between Cu species and surface oxygen vacancies (catalyst redox properties) are believed to have a pronounced and positive effect on catalyst activity for the WGS reaction and other catalytic applications (Djinovic et al; 2008).

Earlier, Au/Al catalysts had been investigated but were shown to have poor activity for the WGS reaction (Lenite et al; 2011). Therefore, gold, originally thought to be inactive for WGS reaction was considered. Addition of gold nanoparticles to metal oxide (CeO_2, Fe_2O_3, TiO_2, ZnO, ZrO_2) supports have yielded positive results for the WGS reaction (Lenite et al; 2011; Kim et al; 2005; Idakiev et al; 2004; Mendes et al; 2008; Andreeva et al; 2002; Andreeva et al; 1996; Andreeva et al; 1996). Ceria (CeO_2), in particular, has been extensively studied as a support material for gold-based catalysts due to its unique and favorable characteristics. It is crucial to control the particle size of both the metal and the ceria support in all preparation methods, because these parameters largely influence the catalytic activity of the system (Fu et al; 2004). Soria et al. (2014) studied the effect of synthesis method on the catalytic activity and stability of Au/Fe_2O_3 catalysts (Table.2.1) for low temperature WGS reaction. Different preparation methodologies such as deposition-precipitation (DP), liquid phase reductive decomposition (LPRD) and double impregnation method (DIM) were employed to synthesize a series of WGS catalysts with varying Au loadings. For the DP and LPRD series, the authors reported excellent dispersion of gold nanoparticles (2.2-3.1 nm) over the iron oxide surface. However, much larger particle sizes (~6.6 nm) were observed for the DIM series of catalysts. The TPR-H_2 profiles of the catalysts indicated that gold nanoparticles promoted the reducibility of the Fe_2O_3 support and thus enhanced the catalytic activity of the system. The Au/Fe_2O_3 catalyst prepared by deposition-precipitation (DP) method exhibited the highest enhancement in CO conversion percentage.

Addition of rare earth metals, especially lanthanum (La), to ceria supports has been widely investigated (Le et al; 2014). Rare earth metals, in general, are known to possess excellent catalytic properties and when added to a ceria catalyst, they lead to improved thermal stability and enhanced catalytic activity (Le et al; 2014; Wang et al; 2010). Wang et al. (Wang et

al; 2011) synthesized a ceria/zirconia catalyst and doped it with rare earth metals like lanthanum (La), neodymium (Nd), praseodymium (Pr), samarium (Sm), and yttrium (Y) and reported that all of the metals exhibited increased activity and selectivity with La, Nd, and Pr performing the best. Gold/ceria catalysts have also been subjected to rare earth metal doping and both lanthanum (La) and gadolinium (Gd) have shown increased catalytic activity (Fu et al; 2005). Jiang et al. (2013) found that yttrium (Y) and lanthanum (La) doping on Cu/Ce/Zr exhibited an increase in OSC over pure ceria, and was further improved with the addition of Fe promoters. Hla et al. (2013) synthesized a CeO_2-La_2O_3-based Cu catalyst (CE09) *via* urea gelation-co-precipitation (UGC) method (Table.2.1) and studied its kinetics for the WGS reaction at two different reaction temperatures: 550 and 600^0C. It was observed that the reverse WGS reaction was less prominent with CE09 catalyst compared to commercial Fe-based HT and Cu-based LT catalysts.

Ceria has a tendency to stabilize carbonate on its surface and this could be inhibited by adding another metal which does not stabilize carbonate formation (Le et al; 2014; Hilaire et al; 2001). One such favorable metal is zirconium (Zr). The addition of zirconium to ceria results in a much higher surface mobility and provides more oxygen transfer sites which enable the reducing effect to be transmitted to molecules deeper in the material (Wang et al; 2010). Zirconium facilitates lower-energy bonding between oxygen molecules when compared to pure ceria (Le et al; 2014). These oxygen molecules are weakly bonded and hence, allow for higher reducibility and thereby higher oxygen storage capacity (OSC), which has been found to be critical to the performance efficiency of the WGS reaction catalyst (Dutta et al; 2006). The effect of preparation method on OSC was also examined and it was reported that a catalyst with a Zr to Ce ratio of 1/3, and precipitated from hydroxides, resulted in higher conversion (Hori et al; 1998; Letichevsky et al; 2005). Novel gold catalysts supported on ZrO_2-modified ceria were also fabricated (Table.2.1) and tested for low-temperature WGS reaction (Vindigni et al; 2012). The

CeO_2-ZrO_2 supports were synthesized by co-precipitation method and then gold particles were introduced *via* deposition/precipitation method. It was reported that the addition of gold nanoparticles to ZrO_2-modified ceria supports enhanced the catalytic activity for WGSR, compared to pure ceria supports. The $AuCe_{50}Zr_{50}$ catalyst was found to exhibit the highest activity and stability due to the high percentage of gold dispersion, along with favorable modifications to the acid/base surface properties of ceria. Wheeler et al. (2004) investigated the possible use of noble metals and other metals with ceria in the temperature range of 300-1000^{0}C and reported the activity of the metals in the order: Ni >Ru> Rh >Pt> Pd. Phatak et al. (2007) studied the effect of Pt supported on alumina and ceria catalysts at different compositions. Gonzaleza et al. (2010) investigated Pt catalysts supported on TiO_2, CeO_2 and Ce-TiO_2 and found that the Pt supported on ceria modified TiO_2 support exhibited better activity than those corresponding to individual ceria and titania supported catalysts. Jeong et al. (2013) synthesized Pt/CeO_2, Pt/ZrO_2 and Pt/$Ce_{(1-x)}Zr_xO_2$ catalysts (Table.2.1) and investigated their applicability for single-stage WGS reaction. Pure CeO_2, pure $ZrO_2$and $Ce_{(1-x)}Zr_xO_2$ supports were prepared by co-precipitation/digestion method and platinum was incorporated *via* incipient wet-impregnation method. Experimental results indicated that the catalytic activity was mainly influenced by the reducibility of the catalyst and partly depended on the percentage dispersion of Pt nanoparticles. Among all the prepared samples, the Pt/CeO_2 nanocatalyst exhibited the highest turnover frequency (TOF) and the lowest activation energy, along with stable activity, in a single stage WGS reaction. Furthermore, Pt supported on cubic $Ce_{(1-x)}Zr_xO_2$ exhibited higher TOF than Pt supported on tetragonal $Ce_{(1-x)}Zr_xO_2$. More recently, Jeong et al. (2015) conducted a comparative study to understand the effect of cubic/tetragonal structure of CeO_2-ZrO_2 support on the activity of catalysts for WGSR. Cubic Cu-$Ce_{0.8}Zr_{0.2}O_2$ and tetragonal Cu-$Ce_{0.2}Zr_{0.8}O_2$ catalysts (Table.2.1) were synthesized *via* co-precipitation/digestion method and their catalytic activity

was investigated at a high gas hour space velocity (GHSV) of 72152 hr^{-1}. It was observed that the cubic Cu-$Ce_{0.8}Zr_{0.2}O_2$ catalyst had a much higher concentration of reduced Cu species than the tetragonal Cu-$Ce_{0.2}Zr_{0.8}O_2$ catalyst. This resulted in strong interaction between Cu and the cubic $Ce_{0.8}Zr_{0.2}O_2$ support, which in turn increased the catalyst's resistance to sintering. The cubic Cu-$Ce_{0.8}Zr_{0.2}O_2$ catalyst was also found to exhibit higher CO conversion (17.4% at 320^0C) than the tetragonal Cu-$Ce_{0.2}Zr_{0.8}O_2$ catalyst, due to its improved oxygen mobility and higher percentage of Cu dispersion.

It is evident that the present research scenario is dominated by ceria based WGS catalysts. The current research modus operandi involves incorporating different metals and metal oxides over a ceria support or synthesizing metal-ceria composites over a different support material which possesses a large surface area. In line with this trend, most of the future research is expected to focus on ceria based catalysts for application in WGS reaction.

2.2.4. Carbon based Water Gas Shift Catalysts:

Yu et al. (2006) developed a catalyst by doping char (the coal gasification product) with iron. It was observed that during the course of the reaction, magnetite (Fe_3O_4) forms in the iron sample and subsequently catalyses the WGS reaction to occur at temperatures just above 300^0C. The main advantages of this catalyst are low cost of production and ease of disposal by re-gasification, during which much of the iron can be recovered. However, presence of sulfur compounds can considerably deactivate the catalyst. Serrano-Ruiz et al. (2008) used an impregnation method to deposit CeO_2 on activated carbon (AC) supports (Table.2.1) and reported extremely high particle dispersion and very small particle sizes (2-4 nm). Buitrago et al. (2012) investigated Pt/Ce on carbon supports and found that the catalyst showed better activity than pure Pt/Ce at high temperatures. The catalyst achieved 90% CO conversion at 350^0C and the activity didn't decrease appreciably even after over 120 h of use.

The Mo/C catalysts have been found to have higher catalytic activity and better sulfur tolerance than conventional catalysts, and no deactivation was observed for 48 h (Oyama et al; 2012; Patt et al; 2000). Also, Pt/Mo/C catalysts were found to exhibit better activity than Pt/TiO_2 and Pt/CeO_2 catalysts; this is due to an increased number of active sites around Pt particles (Schweitzer et al; 2011). The Mo/C catalysts also get deactivated due to change in the states of Mo molecule on the catalyst surface (Moon et al; 2004).

Recently, carbon nanotubes (CNTs) were also investigated as support materials for low temperature WGS catalysts. Zugic et al. (2014) synthesized sodium-promoted platinum catalysts (Table 2.1) supported on multi-walled carbon nanotubes (MWCNTs). The MWCNTs were oxidized by nitric acid and then sodium was introduced by the ion-exchange technique, as per the methodology employed by Roman-Martinez et al. (1994). Platinum was incorporated into the MWCNT support *via* the incipient wetness impregnation method. The authors reported that the catalyst underwent a mild activation for WGSR due to the nitric acid oxidation of the MWCNTs, prior to platinum addition. Also, the incorporation of sodium *via* ion-exchange substantially increased the catalytic activity by altering the surface oxygen distribution. Thus, the promotional effect of Na on CNT-supported Pt catalyst was experimentally verified. Previously, such effects had been reported only for metal-oxide supports(Pigos et al; 2007; Panagiotopoulou et al; 2009; Zhai et al; 2010; Pazmino et al; 2012; Wang et al; 2012; Rosenthal et al; 2010; Boehm et al; 2002; Pierre et al; 2007).

2.2.5. The Nano-materials as Water Gas Shift catalyst:

In addition to doping, directly fabricated nano-structured materials have also shown to significantly enhance the catalytic activity (Zhou et al; 2005; Mai et al; 2005; Lin et al; 2010; Si et al; 2008). Most of the recent research work is being carried out on fabricating nano-structured composite catalysts involving ceria supports along with transition or noble metals. In the

previous sections, there have been quite a few references to such nano-structured catalysts; however, they will be dealt with in much more detail in this section.

As mentioned earlier, with the addition of suitable promoter elements, Ni/Fe catalysts can prove to be effective for HT-WGS reactions. Meshkani and Rezaei (2014) synthesized nanocrystalline chromium-free Fe/Ni/Al HTS catalysts *via* co-precipitation method, with various Fe/Al and Fe/Ni ratios. The catalyst possessed a high surface area of 177.4m^2/g and an average pore size of 4.3 nm. It was reported that the catalyst with Fe/Al=10 and Fe/Ni=5 ratio exhibited higher activity and stability than the other catalysts. Moreover, due to the formation of inverse spinel Ni-ferrites, CO conversion improved considerably and the Fe/Al/Ni catalysts exhibited better activity than the commercial Fe/Cr/Cu catalysts.

Different transition metals catalyze the WGS reaction *via* different reaction mechanisms. For example, copper supported on ceria and nickel supported on ceria is found to follow the redox mechanism (Gawade et al; 2010; Wheeler et al; 2004; Wang et al; 2006). On the other hand, Barrio et al. (2010) have reported that Ni-Ce nano-material is an active catalyst for hydrogen production *via* formate-carbonate route. To understand the WGS reaction mechanism of Ni-Cu alloy catalyst supported on ceria, Saw et al. (2014) prepared Ni-Cu bimetallic catalyst supported on nano-powder CeO_2 and investigated its catalytic activity and restraint to methanation. They reported that the catalyst with Ni/Cu ratio of 1 (5Ni5Cu/CeO_2) exhibited the highest reaction rate and selectivity for WGS reaction. Moreover, kinetic studies revealed that "one-site carboxyl mechanism" could be the main reaction pathway for the 5Ni5Cu/CeO_2 catalyst, though other reaction mechanisms might still be possible. In recent years, SiO_2, Al_2O_3, CeO_2 and ZrO_2, have been extensively studied as support materials for Cu and Ni nano-catalysts (Jeong et al; 2014; Chen et al; 2014; Rad et al; 2012; Lin et al; 2012). Apart from these, activated carbon (AC) has also been investigated as a support material for monometallic Cu, Ni and

bimetallic Cu-Ni nano-catalysts (Arbelaez et al; 2015). Cu/AC, Ni/AC, Cu-Ni (2:1)/AC and Cu-Ni (1:2)/AC were synthesized (Table.2.1) *via* conventional wetness impregnation method and subsequently tested for medium-temperature range (180-350^{0}C) WGS reaction. It was observed that the catalytic activity increased with increase in the reaction temperature for all prepared catalysts. However, the Cu-Ni (2:1)/AC catalyst exhibited the highest activity (99.4% CO conversion), along with satisfactory suppression of methanation and carbon gasification reactions. The authors also reported the Cu-Ni (2:1)/AC catalyst's performance to be comparable to that of ceria-supported noble metal catalysts and suggested that the decrease in methanation activity was due to the synergy between Cu and Ni in the catalysts.

Recently, titania-supported Mn-Cr bimetallic nano-catalyst (Table.2.1) was also prepared for use in HT-WGS reaction (Farzanfar et al; 2015). The authors needs to be expanded selected an inorganic precursor complex $[Mn(H_2O)_6]_3[Cr(NCS)_6]_2.H_2O/TiO_2$ and synthesized the nanocatalyst by impregnation, co-precipitation and thermal decomposition methods. The Mn-Cr/TiO_2 catalyst prepared by thermal decomposition method was found to exhibit smaller particle sizes, higher BET surface area (141.9 m^2/g) and hence, higher catalytic activity (72.6% CO conversion at 320^{0}C) as compared to those synthesized *via* other methods. Meshkani and Rezaei (Meshkani et al; 2015) fabricated nanocrystalline metal (M)-modified (M= Cr, Al, Mn, Ce, Ni, Co and Cu) ferrite crystals (Table.2.1) by co-precipitation method and investigated the consequent structural and catalytic properties. The main aim was to find a suitable non-toxic substitute for chromium in iron oxide catalysts. The results indicated that the active phase formation of the iron oxide catalyst was significantly aided by the addition of copper. Copper also played a major role in increasing the specific surface area of the resultant catalyst. Moreover, it was reported that Fe-Al-Cu catalyst with Fe/Al=10 and Fe/Cu=5 weight ratios showed the highest catalytic activity for WGS reaction, among all other prepared catalysts. It

was also observed that the catalytic activity declined with increase in calcination temperature due to sintering at higher temperatures. Increasing the steam/gas ratio enhanced the WGS activity, but increasing the GHSV adversely affected the percentage of CO conversion due to relatively lower contact time. In a separate study (Table.2.1), the authors investigated the effect of process parameters such as concentration of the precursor solution, pH, aging time and aging temperature, and calcination temperature on the structural and catalytic properties of the prepared nano-crystalline iron based catalysts (Meshkani et al; 2015). The meso-porous nano-catalysts were synthesized *via* co-precipitation method and subjected to high temperature WGS reaction. Experimental studies revealed that the catalyst was composed of nano-particles having sizes between 10 and 20 nm and the specific surface area of the catalyst varied from 28.2 to 91.1 m^2/g. The increase in the specific surface area was favored by an increase in the pH value, whereas it was adversely affected by increments in the calcination temperature and the concentration of the precursor solution. Highest BET surface areas were observed for certain optimum values of aging time (5 hrs) and aging temperature (60^0C), above which the surface area decreased slightly. It was reported that the catalyst prepared from a precursor solution having a concentration of 0.06M, at pH=10, aging temperature of 60^0C, aging time of 5 hrs, and calcined at 400^0C, possessed the highest catalytic activity and CO conversion compared to other samples. Furthermore, Meshkani et al. (Meshkani et al; 2015) also synthesized nanocrystalline Fe_2O_3-Cr_2O_3-CuO powder (Table.2.1) by using a modified urea hydrolysis method and investigated its catalytic properties for HT-WGS reaction. Due to its nanostructure (crystallite size < 15 nm), the catalyst possessed higher surface area and hence, better activity for WGSR than a commercial catalyst. However, it was found that the BET area decreased with increase in the calcination temperature and consequently the catalytic activity also decreased.

Jain and Maric (Jain et al; 2014) employed Reactive Spray Deposition Technology (RSDT) to synthesize 1 wt. % Pt nano-particles (0.5-2 nm) onto nano-structured ceria support (Table.2.1). The resultant catalyst was studied for WGS reaction in the temperature range of 100-350^{0}C and at atmospheric pressure. Catalytic studies indicated superior activity of the RSDT synthesized nano-catalyst compared to catalysts prepared through sol-gel, co-precipitation and incipient wetness impregnation methods. Nearly 99% CO conversion was achieved at 250^{0}C at a GHSV of 8622 hr^{-1}. The enhanced performance can be attributed to the uniform distribution of Pt nano-particles over the ceria surface and the absence of sintering and agglomeration of Pt nano-particles.

In another recent study (Table.2.1), Pt/CeO_2 nanocatalysts were prepared by an incipient wet impregnation method and the pre-calcination temperature and aging time were optimized for achieving the highest activity for WGS reaction (Jeong et al; 2015). Crystalline cerium hydroxy carbonate (CHC: $Ce(OH)CO_3$) was first prepared by a precipitation/digestion method at room temperature and then it was subjected to thermal decomposition to obtain nano-structured ceria supports. The resultant catalyst exhibited the highest CO conversion (~82%) and the lowest activation energy of 55 kJ/mol at a GHSV of 45515 h^{-1}, when a pre-calcination temperature of 400^{0}C and aging time of 4 h was employed in the synthesis of ceria. Characterization studies indicate that the ceria support is composed of nanocrystalline particles and hence, has a high BET surface area. The Ce-PtO_x species at the surface of the catalyst provide the active sites for the WGSR and these sites are adequately stabilized by the nano-structured ceria support (Roh et al; 2012; Pierre et al; 2007; Jeong et al; 2011; Potdar et al; 2011). This intimate interaction between Pt and ceria in the Pt/CeO_2 catalyst can be put forth as an explanation for the aforementioned results.

The $Au/CeO_2/Al_2O_3$ based nano-catalysts had also been recently investigated for WGS reaction and transition metals such as Fe, Cu and Zn were used as CeO_2 dopants (Table.2.1) to promote the activity of the prepared catalysts (Reina et al; 2015). The supports were prepared *via* co-precipitation method and were subsequently doped with 2 wt. % of metal (Fe, Cu or Zn) oxide. Gold was then deposited over the fabricated supports by direct anionic exchange (DAE) method. The WGS activity of $Au/CeO_2/Al_2O_3$ catalyst was found to be significantly enhanced by the addition of Fe, Cu and Zn to the ceria support. The authors attributed the improved catalytic activity to enhanced redox properties and structural promotion. Both Cu and Zn enhanced the OSC of the primary support, but Zn was found to be the better redox promoter between them. However, Fe was reported to be the best choice for a dopant, since it functioned both as a redox promoter as well as a structural promoter.

Recently, palladium/copper/ceria electrospun fibers (Pd/Cu= 2/10 wt. %) were investigated as WGS catalysts (Table.2.1) and the studies showed that the transition metal incorporated in the ceria lattice facilitated the reduction of energy barriers for oxygen vacancy formation in the lattice and thereby promoted H_2O splitting on the ceria surface (Gibbons et al; 2014). The electrospun nanofibers possessed an average diameter of less than 200 nm and the individual ceria crystallites were less than 15 nm in diameter. The specific surface area of the resultant nanocatalyst increased with the addition of a surfactant to the synthesis solution. However, neither did this modification appreciably enhance the catalyst's activity, nor did it slow down its asymptotic decay. This indicates that the activity of such catalysts is largely influenced by the metal-ceria interactions, rather than just by its BET surface area.

2.3. Summary:

The water gas shift reaction is critical for producing pure hydrogen. The WGS catalyst development activity initially started with the development of conventional iron-chromium

catalysts for high temperature shift reactions and copper-zinc catalysts for low temperature shift reactions. However, these catalysts suffered from certain drawbacks and were unsatisfactory regarding the amount of CO that they were capable of removing. Therefore, over the past two decades, researchers have continuously investigated novel materials, explored different options of metal-support combinations, and different fabrication methods in order to improve upon the current generation of WGS catalysts in terms of stability, applicability and activity at moderate temperatures. Various materials have been studied till date but ceria, in particular, has caught the attention of researchers worldwide because of its excellent oxygen transport capacity and the ability to easily switch between its oxidized and reduced states. With the advent of nano-structured materials, the focus has shifted towards synthesizing nano-catalysts which possess considerably better properties (higher surface area to volume ratio) and show enhanced performance compared to other conventional materials. Nano-catalysts have been prepared *via* diverse methods such as sol-gel, co-precipitation, incipient wetness impregnation, reactive spray deposition, electro-spinning, etc. These preparation methods are being investigated to come out with the most suitable and cost-effective method for the synthesis of WGS catalysts having favorable structural properties. The scope of research in this area is quite vast and a lot of breakthrough studies and improvements can be expected in the near future.

Due to its fluorite structure, the all oxygen atoms in a ceria crystal are in the same plane, allowing rapid diffusion controlled by oxygen vacancies. As the number of vacancies increases, the ease at which oxygen can move around in the crystal increases, allowing the ceria to reduce and oxidize molecules on its surface. It has been shown that the catalytic activity of ceria is directly related to the number of oxygen vacancies in the crystal (Djinovic et al; 2008).It can also be used as a co-catalyst in a number of reactions, including water-gas shift and steam

reforming of ethanol or diesel fuel into hydrogen gas and carbon dioxide, the Fischer-Tropsch reaction, and selected oxidation.

2.4. Objectives of the Present Work:

Over the last two decade researches have investigated various polymeric nanofibres for use as catalyst. Selection of material and method is very important to design the catalyst for specific catalytic application. In nanofibres synthesis by electrospinning, the nucleation of polymer crystals takes place in quenched condition resulting in a structure very different from the equilibrium state. The crystallinity and molecular orientation of polymer chains are generally affecting the catalytic properties of the nanofibres. Most often, the inorganic particles are embedded in polymer matrix or sol-gel coating followed by heat treatment. Based on critical assessment of the available literature published in recent past it is obvious that ceria and copper have good potential as catalyst for WGSR. Compared to particulate catalysts, nano-fiber catalysts give better activity and stability with the extremely high surface-to-weight ratio. They have also high surface area to volume ratio (~1000 m^2/m^3), porosity and BET surface area (100-208m^2/g). There are only few articles available on the use of nano-fibers as catalyst in WGSR. The present study has been planned to prepare nano-fibers of CuO/CeO_2 andinvestigate the efficacy as catalyst for water gas shift reaction to increase the yield of H_2 and decrease the content of CO.

In view of the above discussion and need for a cost effective catalyst it has been planned to prepare nano-catalysts CuO/CeO_2 using electrospinning technique and investigate their catalytic activity:

- Preparation of green nanofibers of ceria and (10-60%) CuO/CeO_2 catalysts with varying composition of copper using an electro-spinning device under optimized conditions.

- Optimization various operating parameters for preparation of CeO_2 and (10-60%) CuO/CeO_2 composite nanofibers.
- Calcination of green nano-fibers under appropriate conditions to obtain CeO_2 and (10-60%) CuO/CeO_2 catalysts.
- Complete characterization of various catalysts using various morphological and structural characterization methods such as BET surface area, XRD, TGA, EDX, FTIR, XPS, SEM etc.
- Catalytic activity of prepared catalysts as a water gas shift reaction using an indigenously designed packed bed reactor.
- Interpretation of experimental results to elucidate the kinetic and thermodynamic parameters of relevance.